

Multi-strand Fibers with Hierarchical Helical Structures Driven by Water or Moisture for Soft Actuators

Chenxue Xu, Zhenlin Jiang,* Tiantian Zhong, Chen Chen, Wanting Ren, Tao Sun, and Fanfan Fu*,||

Cite This: *ACS Omega* 2023, 8, 2243–2252

Read Online

ACCESS |



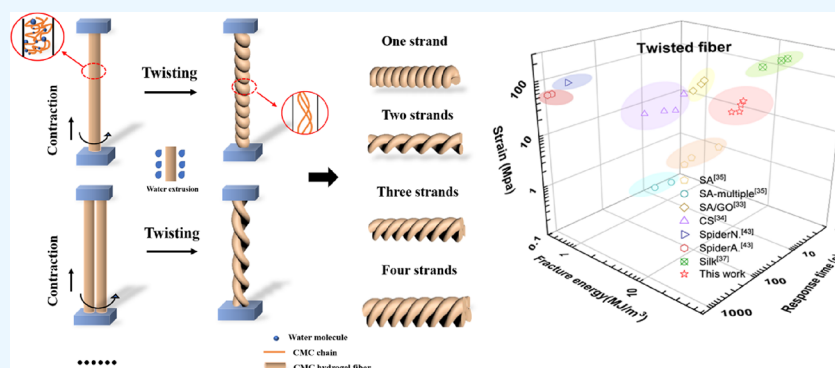
Metrics & More



Article Recommendations



Supporting Information



ABSTRACT: Smart actuators that combine excellent mechanical properties and responsive actuating performance like biological muscles have attracted considerable attention. In this study, a water/humidity responsive actuator, consisting of multi-strand carboxyl methyl cellulose (CMC) fibers with helical structures, was prepared using wet-spinning and twisting methods. The results showed that owing to the multi-strand structure, the actuator consisted of one-, two-, three-, and four-strand helical fibers, thus achieving a combination of high strength (~ 27 MPa), high toughness (>10.34 MJ/m³), and large load limit (>0.30 N), which enable the actuator to theoretically withstand a weight that is at least 20,000 times its weight. Meanwhile, owing to the excellent moisture-responsive ability of CMC, the actuator, with a 5 g load, could achieve untwisting motion. Additionally, its maximum speed was approximately 2158 ± 233 rpm/m under water stimulation, whereas the recovery speed could reach 804 ± 44 rpm/m. Moreover, this untwisting–recovery reversible process was cyclic, whereas the shape and the actuating speed of the actuator remained stable after more than 150 cycles. The actuator improved the load limit that the fiber could withstand when driving under stimulation, thereby enabling the actuator to lift or move heavy objects like human muscles when executing spontaneously under external stimuli. This result shows considerable potential applications in artificial muscles and biomimetic robots.

1. INTRODUCTION

In organisms, a muscle that consists of a bundle of muscle fibers exhibits large load capacity, energy storage, and rapid response to mobility by simultaneous contraction and stretching of multiple muscle fibers.^{1,2} Such a muscle has become a research hotspot for use in imitation and transcendence through flexible actuating materials.^{3–5} Such materials, which can perform reversible motions such as bending, rotation, contraction, and twisting spontaneously in response to external stimuli,^{6,7} such as light,^{8–10} humidity,¹¹ pH,^{12–14} magnetism,^{15–17} and chemicals,¹⁸ have attracted increasing attention for the wide applications of artificial muscles^{19–21} and biomimetic robots.^{22,23} Many materials have been investigated for actuators with high performance, including shape memory²⁴ and conducting polymers, which are made in different forms, such as films,^{25,26} fibers,²⁷ and hydrogels.²⁸ However, although, like living organisms, film and hydrogel actuators can spontaneously respond to external stimuli, their low stability, long response time, poor strength,

and toughness limit their application as strength-requiring actuators.^{29,30} On the contrary, fiber-based actuators that are closest to biological muscles have been of interest to researchers as these actuators leverage strong responsiveness, lightweight, great mechanical properties, and superior flexibility, which enables them to be twisted, knotted, and weaved without any structural failure.³¹

Inspired by the helical structure of plants, fiber-based actuators are usually prepared by introducing an insert twist into the fiber.³² This twist imparts actuating performance to the fiber and also improves its mechanical properties. Biomass-

Received: October 8, 2022

Accepted: November 29, 2022

Published: January 4, 2023



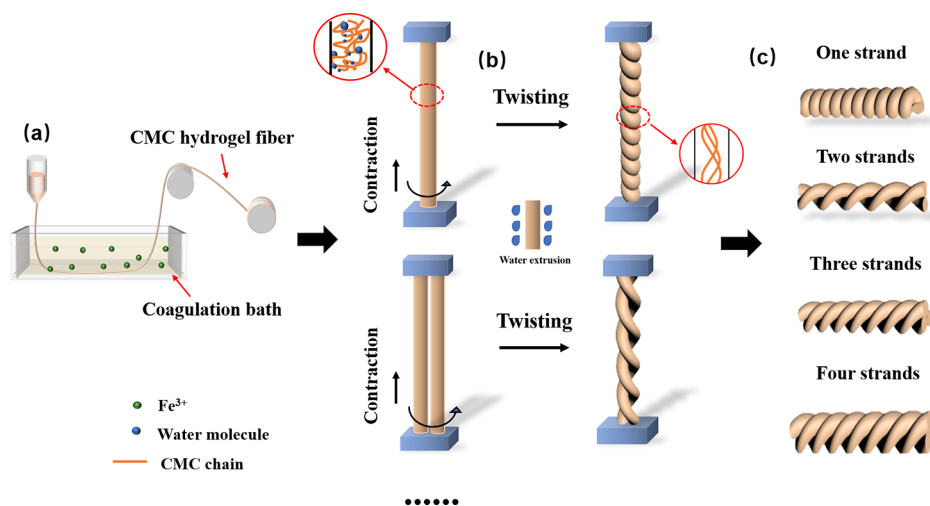


Figure 1. Schematic diagram of the wet spinning and twisting process of the multi-strand CMC fibers with a hierarchical helical structure: (a) wet-spinning method; (b) twisting process of one, two, or more strands of CMC fibers; (c) model diagram of one-, two-, three-, and four-strand hierarchical helical fibers obtained after twisting and setting.

responsive materials are usually used to obtain exciting fiber-based actuators via twisting methods. For example, Zheng et al.³³ introduced a twisted structure into SA/GO fibers as a light-humidity actuator. The strength of the SA/GO fibers improved from 20 to 90 MPa with an increase in the twists, and the maximum rotation speed was 620 rpm. This achieved a combination of actuating performance and enhanced strength. However, the load capacity was low. Chen et al.³⁴ fabricated twisted CS/MWCNT actuators, which showed an excellent response speed to water. However, the toughness of the actuators needed to be improved. An et al.³⁵ mimicked the structure of muscle tissues and fabricated an SA/GO fiber-based actuator by twisting multiple primary SA/GO fibers, which realized a large load capability and a combination of high strength (~ 2 MPa) and toughness (> 5 MJ/m³) in the multi-strand hydrogel fibers. However, the poor responsiveness to the humidity of the actuator with a maximum speed of 7.5 rpm poses a challenge. For a fiber-based silk actuator, which exhibits excellent mechanical properties and has a strength of 400 MPa, its long response time limits its application.³⁶ Thus, it is critical to design an actuator that can realize fast execution speed in response to external stimuli with high strength and good toughness and exhibit large load capability during spontaneous execution.

Carboxyl methyl cellulose (CMC), a bio-based water-responsive material, which has been widely studied as a membrane-based and hydrogel-based actuator, has not yet been introduced into fiber-based actuators.³⁷ Therefore, inspired by the helical structures of plants and muscle tissues, first, a water/humidity-responsive CMC fiber-based actuator, consisting of multi-strand CMC fibers with helical structures, was prepared in this study. We used CMC as a moisture-responsive material, and the helical structure was constructed by orientationally twisting the hydrogel CMC-stranded fibers obtained by wet-spinning owing to the fact that the actuator could rotationally respond to water/moisture.^{38–43} Then, the absorption and desorption of water molecules between the fibers and environment under water/moisture simulation generated the difference between the swelling and torque forces. This difference finally determined the rotation speed in the untwisting–recovery process of the actuator. In addition,

an increase in the fiber strands improved the load limit that the fiber could withstand when driving under stimulation. Consequently, like humans, the actuator could lift or move heavy objects when executing spontaneously under external stimuli. Therefore, the results have a wide application in artificial muscles and biomimetic robots.

2. EXPERIMENTAL SECTIONS

2.1. Materials. The sodium carboxymethyl cellulose (CMC-Na/CMC, DS = 2.5) and ferric chloride hexahydrate ($\text{FeCl}_3 \cdot 6\text{H}_2\text{O}$) were purchased from Sinopharm Chemical Reagent Co., Ltd. (Shanghai, China).

2.2. Synthesis of the CMC Spinning Solution and the Ferric Chloride Hexahydrate Coagulation Bath. First, the CMC powder was put into a beaker, then deionized water was added, the mixture was mechanically stirred for 4 h at room temperature, and the rotation speed was adjusted to 1000 rpm to obtain a stable and uniform 3, 5, or 7 wt % CMC spinning solution.

Deionized water was added to sufficient ferric chloride hexahydrate ($\text{FeCl}_3 \cdot 6\text{H}_2\text{O}$) powder to produce 2, 8, or 14 wt % solutions and stirred at room temperature until the powder had completely dissolved to produce coagulation baths.

2.3. Preparation of the Multi-strand Hierarchical CMC Fibers. The primary hydrogel CMC fiber was formed by the wet-spinning method, the solution was transferred into the syringe, and the solution was extruded at a uniform speed (about 0.10 mm/s) into the coagulation bath. The fiber was removed after molding for approximately 5–10 s. Then, many multiple primary fibers with the same size and length were selected; one end of the fiber was fixed, while the other end was connected to the twisting machine. The twist number of the machine was set to 2500 turns/min. During the twisting process, when the fiber moisture is continuously squeezed out, the fiber diameter becomes smaller and the length becomes shorter accordingly. After twisting, the fibers of 2500 turns/m composed of one-, two-, three-, and four-strand fibers with a helical structure were obtained, and then they were fixed in a dry environment for about 0.5 h to maintain the twist and were stored at a constant temperature (35 °C) and humidity (40RH %) finally.

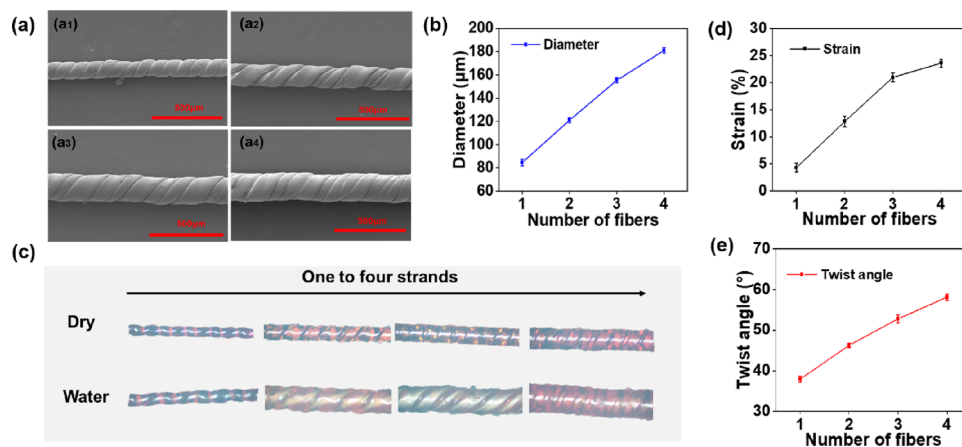


Figure 2. Morphology characterization of the multi-strand hierarchical CMC fibers. (a) Morphology of multi-strand hierarchical helical CMC fibers: (a₁–a₄) one- to four-strand CMC hierarchical helical fibers. (b) Diameter of one- to four-strand CMC hierarchical helical fibers. (c) Optical microscopy diagrams of multi-strand helical CMC fibers before and after the immersion of water. (d, e) Effect of twisting on multi-strand CMC hierarchical helical fibers: (d) twist angle and (e) strain.

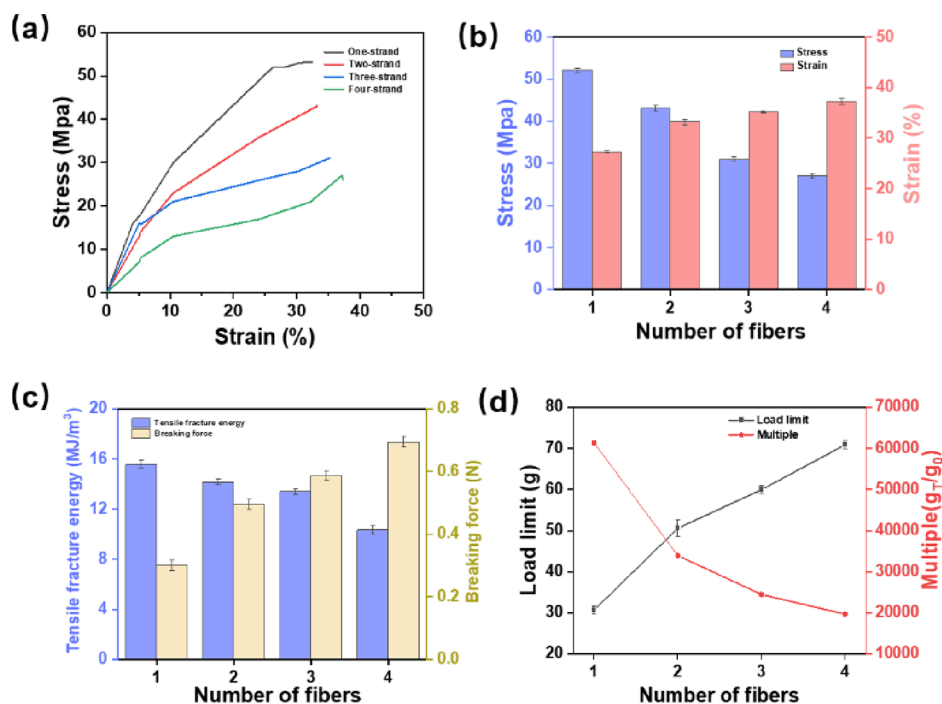


Figure 3. Tensile properties of the multi-strand hierarchical CMC fibers: (a, b) typical stress–strain profiles, (c) fracture energy and breaking force, and (d) load limit.

2.4. Characterization. The morphology of multi-strand fibers with a helical structure was characterized by scanning electron microscopy (SU8010) and optical microscopy (BH200M). The tensile strength of multi-strand fibers was tested by an electronic fabric strength machine (XS (08) XS-2). The changes in the internal structure of CMC in the multi-strand helical fibers before and after water stimulation were detected by low-field NMR (PQ001). The actuating performance of the fibers in response to water/moisture simulation was investigated by spraying water on the texted fibers or adjusting the relative moisture in a homemade sealed glass container with an ultrasonic humidifier (HQ2008A6) and a hygrometer (Anymetre JR916); the texting results were recorded by an infrared tachometer and a non-contact laser counter. The

experimental data and corresponding errors were analyzed by the method of averaging multiple measurements.

3. RESULTS AND DISCUSSION

3.1. Morphology Characterization and Tensile Properties of the Multi-strand Hierarchical Helical CMC Fibers. To fabricate the multi-strand CMC fibers with a hierarchical structure, a method of wet-spinning combined with directional twisting was employed. As shown in Figure 1a, when the spinning solution slowly enters into a coagulation bath that is filled with Fe³⁺, a rapid cross-linking reaction is initiated by Fe³⁺, forming a single-strand CMC hydrogel fiber with high water content accordingly. Then, many multiple primary fibers with the same sizes and lengths, which were prepared by using a uniform type of 27-gauge needle, were

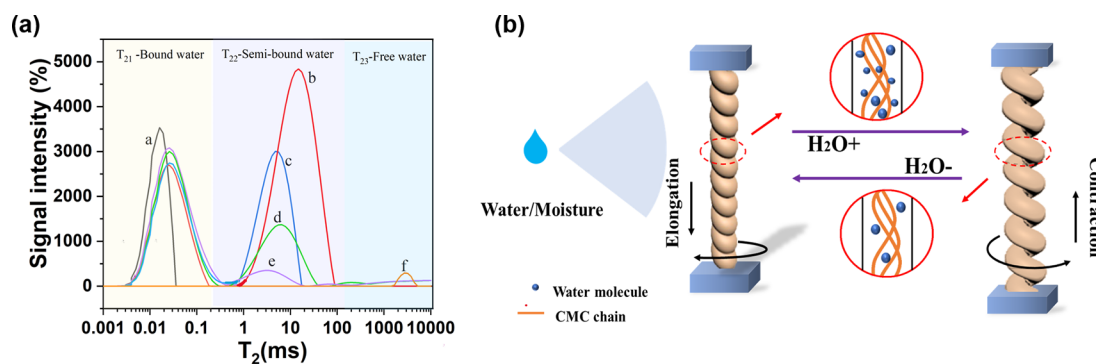


Figure 4. Mechanism explanation of actuating performance of multi-strand helical CMC fibers under water stimulation: (a) low-field NMR images of the multi-strand before and after being stimulated by water (a: the initial that is not soaked in deionized water; b–e: the multi-strand helical CMC fibers that is soaked in deionized water and dried for 0, 30, 60, and 120 s; and f: deionized water) and (b) mechanism diagram of actuating performance of multi-strand helical CMC fibers under water stimulation.

selected. One end of the fiber was fixed, while the other end was connected to the twisting machine, as shown in Figure 1b. The twisted fibers exhibited 2500 turns/m and comprised one-, two-, three-, and four-strand fibers with a helical structure. They were obtained by directional twisting of multiple single strands, as shown in Figure 1c. During the twisting process, as the water molecules in the fibers were continuously extruded, both the fiber diameter and length decreased. Moreover, the long CMC chains changed from a disordered and loose state to a regular and compact state, as shown in Figure 1b.

Scanning electron microscopy was used to characterize the morphology of the multi-strand fibers, as shown in Figure 2a. Notably, the surfaces of the CMC fibers were covered with neat threads under the action of a twisting force, exhibiting a distinct helical structure. Moreover, as the number of fiber strands increased, the diameters of fibers in the same twists increased from 84.67 ± 0.63 to 181 ± 1.01 μm , as shown in Figure 2b. The reason is that, although the water of the twisted fibers was extruded during the twisting process, causing a decrease in diameter, the diameters of multi-strand fibers with the same twists were primarily determined by the fiber strands that participated in the twisting. Figure 2c shows the optical microscopy diagrams of the multi-strand helical CMC fibers before and after the immersion of water. An increase in diameter and a decrease in the threads of spiral structures were observed under the effect of water owing to the excellent moisture absorption ability of CMC fibers compared with that of dry fibers. Meanwhile, the expansion of the fiber also increased with an increase in the number of strands because the hygroscopic component increased, increasing the moisture absorption capacity of the fiber. Interestingly, we found that such twisted multi-strand fibers with a helical structure shown in Figure 2a can be made more compact with the strand of the fibers increased from one to four. This can be confirmed by the variation in the twist angle and shrinkage rate, as depicted in Figure 2d,e. Notably, as the number of fiber strands increased from one to four, the twisted angle changed from $37.9^\circ \pm 0.6$ to $58.1^\circ \pm 1.3^\circ$, and the shrinkage rate increased from 5 ± 0.67 to $23.6 \pm 1.93\%$. This could be explained by considering the stack of the helical structure. Specifically, compared with a single twisted fiber, multi-strand fibers with the same twists can be regarded as a twisted stack of each single strand inside. Consequently, the internal structure of the fiber was relatively dense and more compact.

However, although an increase in the number of strands renders the helical structure of the fiber with the same twist more compact, its mechanical properties are decreased compared with that of a single fiber. Figure 3a,b shows the tensile test results. Notably, the strain of the fiber increased slightly, whereas its stress decreased significantly as the number of strands increased. The maximum strain was 53.4 MPa for a single strand, whereas it was 27 MPa for four-strand fibers. This difference can be attributed to the tiny gaps between adjacent strands when multiple fibers are twisted together, weakening the fiber strength. The fiber strain tended to increase within the range 32.4–37.3% with different strands. The fracture energy of the multi-strand fibers was obtained by calculating the area of the stress–strain curve, as shown in Figure 3c. Herein, the fracture energy and stress of the fibers have the same changing tendency. The variation range increased considerably from 10.34 to 15.56 MJ/m^3 . Conversely, with an increase in the number of fiber strands, the maximum load that the fiber could withstand increased significantly from 0.30 ± 0.0002 to 0.69 ± 0.0001 N, as depicted in Figure 3c. This figure shows that, compared with single-strand fibers, multi-strand fibers can lift heavier objects. Theoretically, the load limit of fibers with different strands can be calculated and it exhibits the same trend as the maximum load that increases with the number of strands ranging from 30.68 to 70.89 g, which is calculated by substituting the maximum stress value into the formula $F = mg$ as shown in Figure 3d. Therefore, a multi-strand fiber can theoretically withstand a weight that is at least 20,000 times its weight.

3.2. Actuating Properties of the Multi-strand Hierarchical CMC Fibers under Water Stimuli. Owing to the presence of moisture-responsive CMC materials with many oxygen-containing functional groups such as hydroxyl and carboxyl in the molecular chain, multi-strand helical CMC fibers can be applied as water/moisture actuators. To further investigate the changes in CMC structures under water stimulation, low-field nuclear magnetic resonance was used to analyze the multi-strand helical CMC fibers, which had undergone 0, 30, 60, and 120 s after immersion into deionized water for 5 s. The deionized water and dry fibers were also tested as references. The range of values of T_2 in the inversion spectra are T_{21} (0.001–0.1 ms), T_{22} (0.1–100 ms), T_{23} (1000–10,000 ms), which represent “bound water”, “semi-combined water”, and “free water”, respectively. The results showed that the CMC fibers exhibited excellent reversible

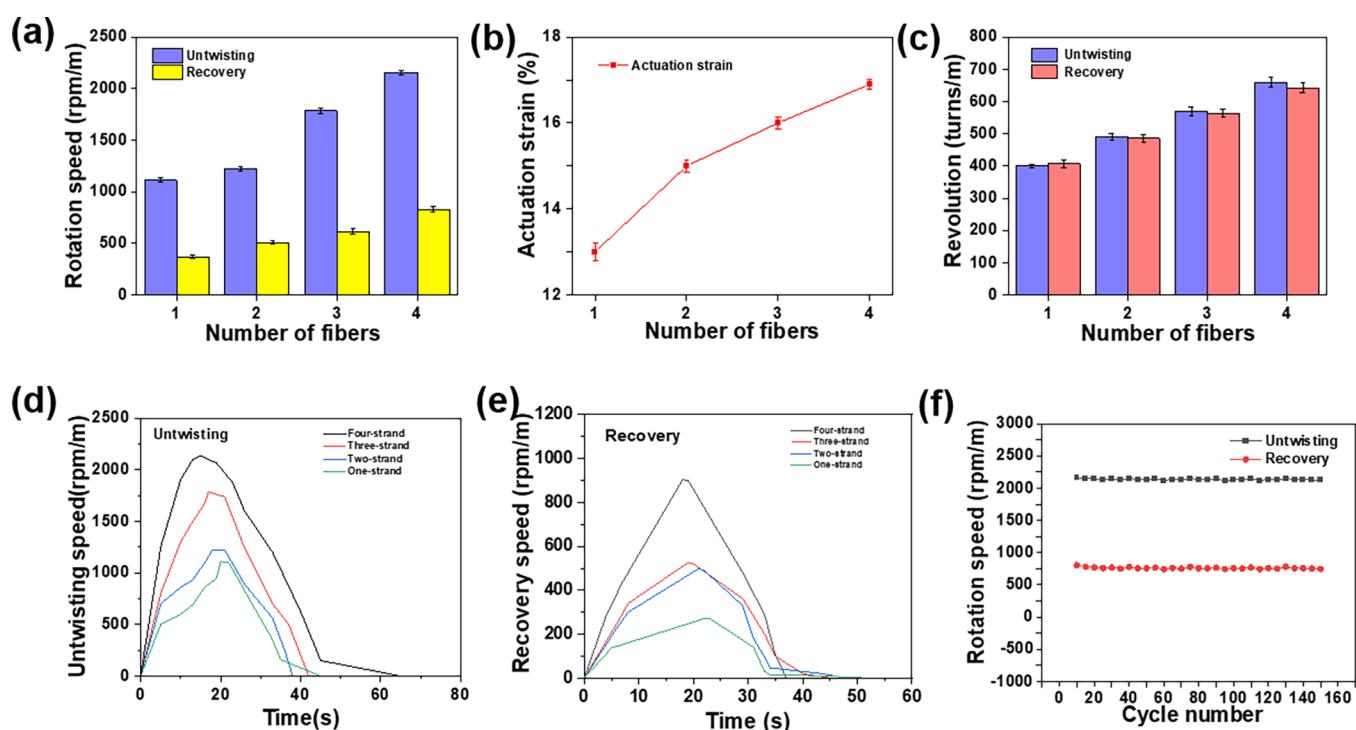


Figure 5. Comparison of actuating performance of multi-strand helical fibers under water stimulation: (a) rotation speed, (b) actuation strain, (c) revolution, (d) record of the untwisting process of actuating speed over time, (e) record of the recovery process of actuating speed over time, and (f) rotational stability of the four-strand helical fiber with a 2500 turn/m twist under water stimulation.

water adsorption and desorption properties. In detail, the signal of the dry fiber was the strongest in the bound water region of T_{21} , as depicted in Figure 4a. This indicated that the oxygen-containing functional groups and water inside the fiber had formed stable bound water. However, after immersing in water (b curve in Figure 4a), the signal value of the bound water of the fibers was lower than that of the dry fibers (a curve in Figure 4a). This was because the addition of free water caused some of the bound water with high mobility inside the fibers to gradually turn into semi-bound water, which could be confirmed by an increase in the signal of T_{22} .

With an increase in the drying time of the fibers, the signal value of the fibers in T_{22} gradually decreases (b–e curve in Figure 4a). Conversely, the other semi-bound water, owing to the deterioration of fluidity, gradually migrated to the bound water, causing the signals in T_{21} and T_{22} to slowly return to their initial states. This process demonstrates that water molecules have good mobility in the CMC chain, enabling reversible, adsorption–desorption behavior.

Owing to the excellent hygroscopic properties of the CMC and the unique layered helical structure of the twisted fibers, the dynamic reversible adsorption and desorption behavior between the water molecules and multi-strand fibers can be established, as revealed in Figure 4b. Notably, when water is stimulated continuously, the volume of fiber expands owing to the rapid absorption of water with a significant volume expansion, thereby generating a considerable swelling force to promote the untwisting of the fibers. The fiber rotates in the direction of untwisting until the swelling force exceeds the torque force imparted by twisting, during which the fiber length is elongated. Conversely, as soon as the water stimulation stops, the water molecules inside the fiber evaporate rapidly. Consequently, the swelling force decreases, and the twisted fiber recovers its original state owing to the

rotation along the twisting direction dominated by the torque force.

To further test the effect of the number of fibers on the untwisting speed and recovery speed in response to water or humidity stimulation, 10 cm fibers with different strands were chosen. Figure 5a shows the untwisting and recovery speeds of the fibers. The results showed that with an increase in the number of fiber strands from one to four, the untwisting speed increased linearly, ranging from 1111 ± 102 to 2158 ± 233 rpm/m. In the meantime, the recovery speed, although numerically less than the untwisting speed approximately three times, had the same changing trend. The speed difference can be explained by the fact that the evaporation rate of water molecules at room temperature is slower than their absorption and diffusion rate. Moreover, in a four-strand fiber, the maximum value of the recovery speed was 804 ± 44 rpm/m. The reason is that the swelling force generated by the water absorption of the fiber increased as the number of fiber strands increased, thereby accelerating the speed. Moreover, the rate of water desorption also slowed down accompanied by an increase in the amount of water inside the fibers.

Additionally, the elongation changed from 13 to 16.9%, and the full revolutions (the number of turns performed by the fibers swirling under water stimulation) were increased to 660 turns/m during water stimulation, as depicted in Figure 5b,c, respectively. These changes can also be attributed to an increase in the swelling force of the fibers caused by changes in fiber strands under water stimulation. Figure 5d,e shows the entire untwisting–recovery process of the multi-strand helical CMC fibers under water simulation. Notably, after 5 s of water stimulation, the rotational speed increases almost linearly and rapidly within actuating time and the revolution also increases rapidly. Herein, we defined the time to reach the fastest response speed as the response time. Figure 5d shows that

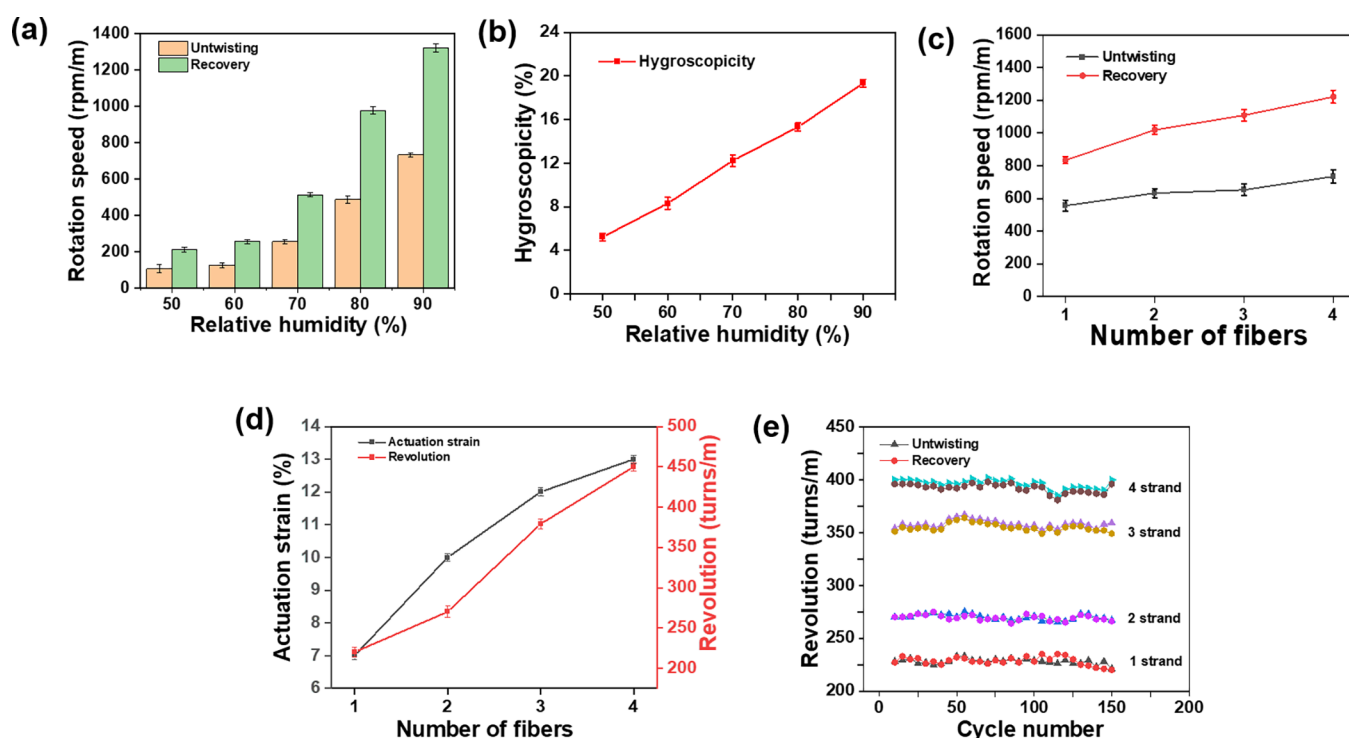


Figure 6. Comparison of actuating performance of helical fibers with different strands under changing moisture stimulation: (a) rotation speed of four-strand helical fibers under different humidity conditions, (b) hygroscopicity of four-strand helical fibers under different humidity conditions, (c) rotation speed of helical fibers with different strands under high RH90% and low RH40%, (d) record of the untwisting process of actuating strain and revolutions over time of the four-strand helical fiber with a 2500 turn/m twist (RH90%), and (e) rotational stability of the four-strand helical fiber with a 2500 turn/m twist under high RH90% and low RH40%.

fibers with four strands exhibited the best actuation performance within 15 s of response time only during the untwisting process. Moreover, the response time decreased as the number of strands increased, which could be attributed to the mechanical energy stored in the twisting process. During the twisting process involving multi-strand fibers with the same twists, the shrinkage strain increased with an increase in the number of strands. Consequently, the stored mechanical energy increased and subsequently enabled the fibers to reach a high driving speed within a relatively shorter time. In addition, as the moisture absorption rate decreases, the speed gradually decreases from the maximum value, and the fiber continues to rotate until 65 s, where a moisture absorption balance is temporarily reached. The response time of the recovery process of the same fiber is longer than that of the untwisting process because more time was required to desorb water molecules, as depicted in Figure 5e. In addition, the repeatability test results, shown in Figure 5f, reveal that such reversible actuating performance of fibers is stable whose speed exhibited no downtrend after 154 times of stimulation.

3.3. Actuating Properties of the Multi-strand Hierarchical CMC Fibers under Moisture Stimuli. To investigate the driving performance of the multi-strand fibers under humidity stimulation, the rotation speed of a 10 cm four-strand fiber under different ambient humidities was recorded, as shown in Figure 6a (the moisture in the air was RH40%). Notably, the speeds of the untwisting and recovery processes increased accordingly as the humidity increased from 50 to 90%. The reason is that, as the humidity increased, the fibers absorbed more water molecules and swelled. Furthermore, as the moisture increased to 90%, the hygroscopicity of the fiber increased from 5 to 24%, as shown in Figure 6b,

confirming the aforementioned explanation for the speed increase. Conversely, the recovery speed changed significantly from 214 ± 23 to 1321 ± 101 rpm/m and approximately doubled the untwisting speed, whose variation ranged from 107 ± 11 to 734 ± 32 rpm/m. This was primarily because moisture in the air penetrated the fibers at a slower rate during the untwisting process, resulting in a slower rotational speed. Meanwhile, when the moisture-laden fibers in high-humidity environments entered a low-humidity environment, a huge moisture gap was established between the fibers and air. Thus, the water molecules in the fibers precipitated rapidly, thereby accelerating the movement of the fibers. Figure 6c shows the relationship between the rotational speed and fiber strands, in which RH90% and RH40% are considered high- and low-moisture environments, respectively. In contrast to water stimulation, the recovery speed under moisture stimulation is faster than the untwisting speed, which is due to the direct adsorption of water molecules by fibers during water stimulation, and the moisture in the air in the humidity environment is slowly diffused to the surface of the fiber by means of penetration, resulting in a smaller swelling force required for untwisting and slower untwisting drive. On the contrary, when the saturated aqueous fibers that achieve moisture absorption balance in a high-humidity environment enter the low humidity environment, a huge humidity difference will be formed between the fibers and the low-humidity air, which makes the water molecules in the fibers precipitate rapidly, thereby accelerating the twisting recovery movement of the fibers. As the number of fibers increased from one to four, the untwisting speed increased; however, it was approximately twice less than the recovery speed. Figure 6d shows the effect of the fiber strands on the strain and

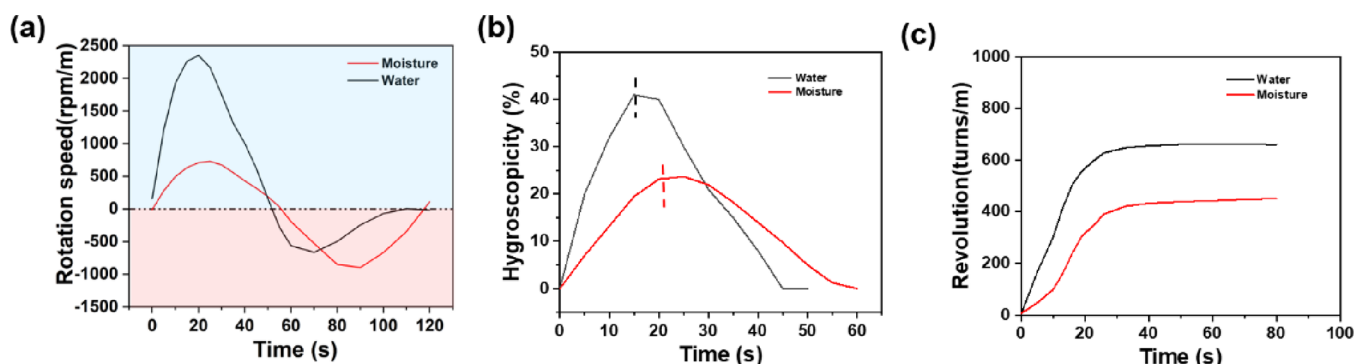


Figure 7. Performance comparison of multi-strand fibers under water or moisture stimulation: (a) rotation speed of four-strand helical fibers in the untwisting–recovery process, (b) hygroscopicity change of four-strand helical fibers in the untwisting process, and (c) revolution change of four-strand helical fibers in the untwisting process.

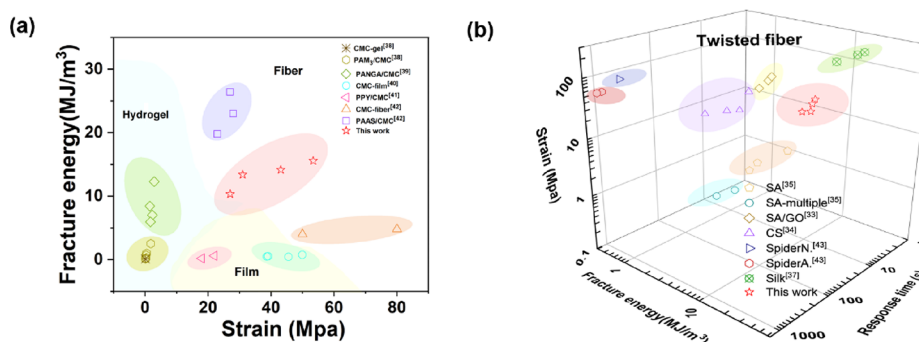


Figure 8. Comparison and summary of response characteristics of existing bio-based actuators: (a) mechanical properties of membrane, fiber, and hydrogel actuators based on CMC and (b) three-dimensional plot of the response time, fracture energy, and strain for bio-based twisted fiber actuators.

revolution during the untwisting process under RH90%. Herein, the elongation increased from 7 to 13%, and the revolutions from 220 to 450 turns/m. Additionally, the cyclic stability of the fibers was tested by the number of revolutions during the rotation process, as shown in Figure 6e. Herein, the revolution of the fibers was unchanged after more than 150 moisture stimulations, showing a stable execution ability.

Figure 7a summarizes the process including the untwisting and recovery performances of the four-strand helical fibers, in which we compare the rotational speed through a simulation with both water and a high humidity of 90%, respectively. The results showed that, although the trend of the speed changed, the process exhibited extreme similarities. For example, in the case of the water simulation, the untwisting speed was approximately twice what it was under the moisture condition. Conversely, a complete reversal of such difference occurred in the recovery process, i.e., the recovery speed under RH90% was higher than that under the water simulation. This indicated that the rotational speed of the fibers may be determined by the absorption and desorption rates of the water molecules. This claim is depicted by the hygroscopicity of the fibers in the untwisting process shown in Figure 7b. Notably, the fibers reached saturation at a steady speed in the water, and the maximum hygroscopicity of the fibers was approximately 40%, which was significantly higher than that in moisture, corresponding exactly to the speed change shown in Figure 7a. Additionally, the response time under moisture stimulation is longer than under water, which is because moisture enters the fiber through water vapor penetration, compared to water stimulation under which water directly enters the fiber,

speed is slower, and it takes more time for the fiber to reach the swelling degree when driving, so the response time becomes longer.

In addition, the revolution also showed the same difference in Figure 7c. The lower hygroscopic rate under the moisture stimulation compared to water stimulation resulted in less fiber swelling, which in turn resulted in a fold difference in the rotational speed and revolutions between both conditions.

3.4. Response Characteristics of Soft Actuators.

Actuators with artificial structures and forms are obtained to achieve excellent mechanical properties such as high strain, toughness, and actuating performance. The mechanical properties of a CMC-based actuator with different forms (such as films, fibers, and hydrogels) are summarized in Figure 8a. Notably, compared with membranes and hydrogels, whose strain and toughness are higher, as depicted in Figure 8a, fiber-based CMC actuators exhibited more mechanical properties. Among fiber-based CMC actuators, a pure CMC fiber has the highest strain, but its toughness is the lowest. Similarly, a PAAS/CMC fiber has the highest toughness, but its strain is the lowest. Compared with these fibers, our fibers exhibited higher toughness and strength, thus achieving a superior mechanical property. In addition, the mechanics and response time of bio-based twisted fiber actuators were analyzed longitudinally, as shown in Figure 8b. The result revealed that the toughness and strength of our fibers were better than those of SA, SA/GO, and CS twisted fiber actuators, and their response time was closer to those of SA/GO and CS actuators but faster than those of single- and multi-strand SA fibers with the same number of twists. Moreover, although silk actuators

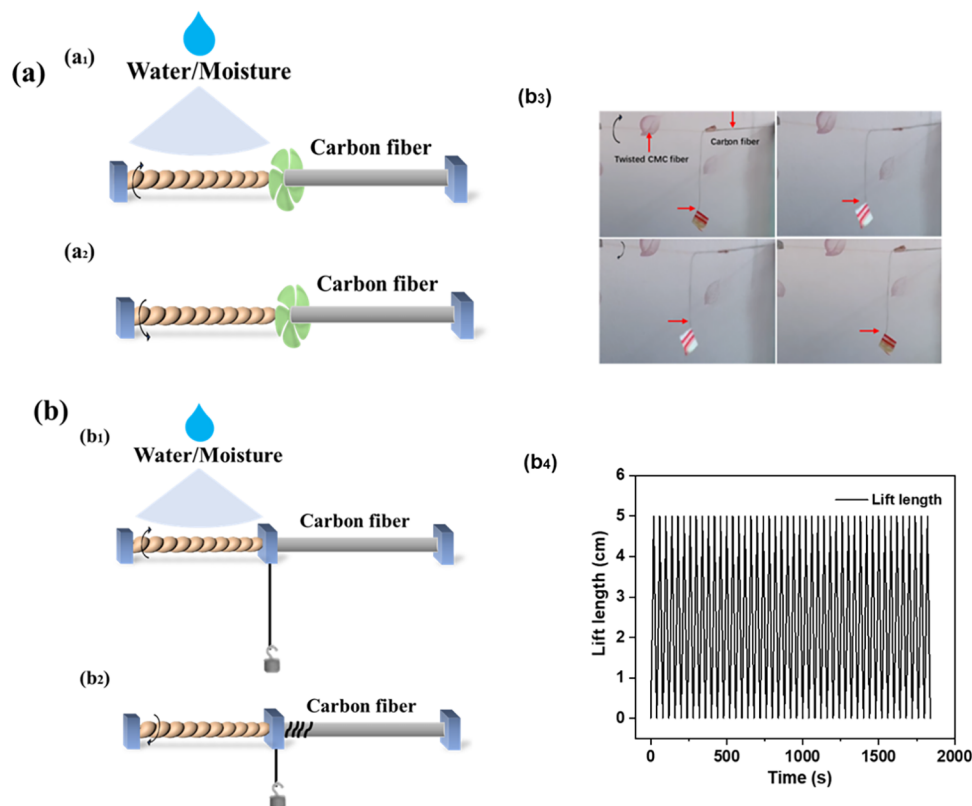


Figure 9. Illustration and physical diagram of the multi-strand fiber-based actuator application: (a) smart fan driven by water or moisture and (b) smart jack driven by water or moisture.

have the highest strain and toughness, their response times are longer than those of other actuators. Therefore, our actuator prepared by multi-strand helical CMC fibers realizes a combination of excellent mechanical properties and responsive actuating performance, which has a wide application in artificial muscles and biomimetic robots.

3.5. Application. Inspired by the excellent mechanical properties and responsive actuating performance of actuators consisting of multi-strand helical CMC fibers under water/moisture stimulation, we realized a moisture-driven fan and smart jack, as shown in Figure 9. We connected CMC fibers to carbon fibers that had not undergone any phenomenon under the water stimulation, and the paper sheets were fixed at the connections. Then, we straightened both ends of the fibers, thus obtaining a simple fan driven by water. The diagram of the mechanism is shown in Figure 9a. When water/moisture was stimulated, the CMC fiber on the left began untwisting and rotated at a high speed, driving the carbon fiber to rotate as a result of stress relief. Consequently, the paper started to rotate continuously like a fan blade (the process is shown in the Supplementary Material, Movie S1). When the moisture on the fiber surface evaporated, the CMC started recovering slowly. The rotational direction during the recovery process was opposite to that during the untwisting process. Finally, the moisture inside the fiber reached equilibrium and stopped rotating. By leveraging the responsive actuating performance of the CMC fibers, it may be applied to humidity/moisture-responsive fans and shutters, which can intelligently be directly driven by the changes in the humidity or moisture on the fiber surface.

In addition, we realized a simple smart jack driven by water/moisture by hanging a 3 g object with carbon fiber at the

connection between the CMC fibers and carbon fiber, as shown in Figure 9b. When the water vapor was sprayed in the CMC section, the distance between the lower end of the suspended object and the fiber was 5 cm (Figure 9b₃). Then, the fibers were untwisted and started to rotate. After approximately 5 s, the carbon fiber connecting the objects began to be wounded owing to the hanging weights on the fibers, and the objects were lifted to a height of 1 cm (Figure 9b₃). Then, all the carbon fibers hanging the heavy object were wounded and lifted the object to a height of 3 cm after 14 s. When the water vapor on the CMC fibers evaporated, the rotation of the CMC fibers was reversed and the object was lowered to its initial height (the process is shown in the Supplementary Material, Movie S2). In addition, when the load of the fiber was increased, the fiber could still carry out lifting heavy objects stably under a heavy load of 50 g that about 14,700 times of its own weight (about 0.0034 g) (the process is shown in the Supplementary Material, Movie S3). Through multiple cycle stimulations, this lifter has good circulation stability and can lift heavy objects about 85 times continuously (Figure 9b₄). Therefore, such CMC fiber actuators can be applied to smart devices like elevator lifts triggered by water or moisture, which is clean and non-polluting. Thus, this validates the promising application of twisted CMC fibers in smart fields.

4. CONCLUSIONS

First, we prepared a water/humidity-responsive actuator consisting of multi-strand CMC fibers with high strength and toughness, exhibiting a helical structure realized by wet-spinning and twisting methods. CMC was used as a moisture-responsive material. The mechanical properties of the actuator

improved by twisting multiple fibers, causing the actuator to withstand heavier weights. Moreover, owing to the excellent water-responsive capability of CMC, the actuators with a helical structure could rotate with a 5 g load in response to water/moisture under the effect of the difference between the swelling and torque forces, which were generated by the absorption and desorption of water molecules between the fibers and environment under water/moisture simulation. Finally, we realized smart fans, which could intelligently be driven directly by the changes in the humidity or moisture on the fiber surface, and smart jacks, which could lift objects by adjusting the strength of the moisture stimulus. Thus, we provided a new concept in intelligent robot fields for the transportation of heavy objects.

■ ASSOCIATED CONTENT

SI Supporting Information

The Supporting Information is available free of charge at <https://pubs.acs.org/doi/10.1021/acsomega.2c06487>.

(Figure S1) Mechanical properties and hygroscopic swelling test of CMC fibers before twisting and (Figure S2) effect of the number of strands on the twist limit (PDF)

Application of the multi-strand CMC helical fiber-based actuator as a smart fan (MP4)

Application of the multi-strand CMC helical fiber-based actuator as a smart jack with 3 g load (MP4)

Application of the multi-strand CMC helical fiber-based actuator as a smart jack with 50 g load (MP4)

■ AUTHOR INFORMATION

Corresponding Authors

Zhenlin Jiang – College of Chemistry and Chemical Engineering, Research Center for Advanced Mirco- and Nano-Fabrication Materials, Shanghai University of Engineering Science, Shanghai 201620, P. R. China; Science and Technology on Advanced Ceramic Fibers and Composites Laboratory, National University of Defense Technology, Changsha 410073, P. R. China; orcid.org/0000-0003-2087-9924; Email: jiangzhenlin@sues.edu.cn

Fanfan Fu – School of Environmental and Biological Engineering, Nanjing University of Science and Technology, Nanjing 210094, China; Email: f3_fanfanfu@njust.edu.cn

Authors

Chenxue Xu – College of Chemistry and Chemical Engineering, Research Center for Advanced Mirco- and Nano-Fabrication Materials, Shanghai University of Engineering Science, Shanghai 201620, P. R. China

Tiantian Zhong – College of Chemistry and Chemical Engineering, Research Center for Advanced Mirco- and Nano-Fabrication Materials, Shanghai University of Engineering Science, Shanghai 201620, P. R. China

Chen Chen – College of Chemistry and Chemical Engineering, Research Center for Advanced Mirco- and Nano-Fabrication Materials, Shanghai University of Engineering Science, Shanghai 201620, P. R. China

Wanting Ren – College of Chemistry and Chemical Engineering, Research Center for Advanced Mirco- and Nano-Fabrication Materials, Shanghai University of Engineering Science, Shanghai 201620, P. R. China

Tao Sun – College of Chemistry and Chemical Engineering, Research Center for Advanced Mirco- and Nano-Fabrication Materials, Shanghai University of Engineering Science, Shanghai 201620, P. R. China

Complete contact information is available at: <https://pubs.acs.org/10.1021/acsomega.2c06487>

Author Contributions

||F.F. contributed equally. The manuscript was written through contributions of all authors. All authors have given approval to the final version of the manuscript.

Funding

This work was financially supported by the Young Science and Technology Talent Sailing Project of Shanghai (grant 19YF1417800).

Notes

The authors declare no competing financial interest.

■ ACKNOWLEDGMENTS

Thanks to the Young Science and Technology Talent Sailing Project of Shanghai (Grant 19YF1417800) for the funding of the project and College of Chemistry and Chemical Engineering, Research Center for Advanced Mirco- and Nano-Fabrication Materials, Shanghai University of Engineering Science, Shanghai 201620, P. R. China for the experimental platform and test instruments and all the authors who have given approval to the final version of the manuscript.

■ REFERENCES

- (1) Wang, Y.; Huang, X.; Zhang, X. Ultrarobust, tough and highly stretchable self-healing materials based on cartilage-inspired non-covalent assembly nanostructure. *Nat. Commun.* **2021**, *12*, 1291.
- (2) Li, X.; Liu, J.; Li, D.; Huang, S.; Huang, K.; Zhang, X. Bioinspired Multi-Stimuli Responsive Actuators with Synergistic Color- and Morphing-Change Abilities. *Adv. Sci.* **2021**, *8*, No. e2101295.
- (3) Rath, B. B.; Gupta, M.; Vittal, J. J. Multistimuli-Responsive Dynamic Effects in a One-Dimensional Coordination Polymer. *Chem. Mater.* **2022**, *34*, 178.
- (4) Kim, S.; Quy, H. V.; Bark, C. W. Photovoltaic technologies for flexible solar cells: beyond silicon. *Mater. Today Energy* **2021**, *19*, No. 100583.
- (5) Wang, Y.; Su, G.; Li, J.; Guo, Q.; Miao, Y.; Zhang, X. Robust, Healable, Self-Locomotive Integrated Robots Enabled by Non-covalent Assembled Gradient Nanostructure. *Nano Lett.* **2022**, *22*, 5409–5419.
- (6) Li, X.; Liu, J.; Li, D.; Huang, S.; Huang, K.; Zhang, X. Bioinspired Multi-Stimuli Responsive Actuators with Synergistic Color- and Morphing-Change Abilities. *Adv. Sci.* **2021**, *8*, 2101295.
- (7) Cao, J.; Zhou, C.; Su, G.; Zhang, X.; Zhou, T.; Zhou, Z.; Yang, Y. Arbitrarily 3D Configurable Hygroscopic Robots with a Covalent–Noncovalent Interpenetrating Network and Self-Healing Ability. *Adv. Mater.* **2019**, *31*, 1900042.
- (8) Bolognari, M.; Mo, A.; Fontana, M.; Badri-Sprwitz, A. Diaphragm Ankle Actuation for Efficient Series Elastic Legged Robot Hopping. arXiv:2203.01595 2022, DOI: 10.48550/arXiv.2203.01595.
- (9) Kodama, Y.; Sakamoto, K. Monocular 3D Display Unit Using Polypyrrole Light-weight Actuator for Image Shift Device. In *International meeting on information display; International display manufacturing conference and Asia display*; IMID/IDMC/Asia Display 2010, 2011.
- (10) Hornig, A.; Froberg, R.; Bätzel, T.; Gude, M.; Modler, N. Embedded sensing and actuating in CFRP composite structures—concept and technology demonstration for tailored embeddable

- sensor-actuator layers (TEmsAL). *Smart Mater. Struct.* **2022**, No. 095007.
- (11) Zheng, Q.; Xu, C.; Jiang, Z.; Zhu, M.; Chen, C.; Fu, F. Smart actuators based on external stimulus response. *Front. Chem.* **2021**, *9*, No. 650358.
- (12) Houben, S. J. A.; Lugger, S. J. D.; van Raak, R. J. H.; Schenning, A. P. H. J. A pH-Responsive Liquid Crystal Hydrogel Actuator with Calcium-Induced Reprogrammable Shape Fixing. *ACS Appl. Polym. Mater.* **2022**, *4*, 1298–1304.
- (13) Kurniawan, D.; Anjali, B. A.; Setiawan, O.; Ostrikov, K. K.; Chung, Y. G.; Chiang, W. H. Microplasma Band Structure Engineering in Graphene Quantum Dots for Sensitive and Wide-Range pH Sensing. *ACS Appl. Mater. Interfaces* **2022**, *14*, 1670.
- (14) Sabelhaus, A. P.; Mehta, R. K.; Wertz, A. T.; Majidi, C. *In-Situ Sensing and Dynamics Predictions for Electrothermally-Actuated Soft Robot Limbs* **2022**, 888261.
- (15) Ding, L.; Zhang, J.; Shu, Q.; Liu, S.; Xuan, S.; Gong, X.; Zhang, D. Magnetism-Responsive Anisotropic Film with Self-Sensing and Multifunctional Shape Manipulation. *ACS Appl. Mater. Interfaces* **2021**, *13*, 13724–13734.
- (16) Chang, Y.-J.; Zhou, Q.; Hou, W.-H.; Liang, Y.-H.; Ren, L.; Sun, D.-H.; Ren, L.-Q. Design and Preparation of Magnetism-Driven Intelligent Hydrogel Actuators. *Int. Polym. Process.* **2021**, *36*, 165–171.
- (17) Weng, G.; Ding, J.; Wu, Y.; Liu, Y. Magnetism-mechanics Performance of Magnetically Controlled Shape Memory Alloy and Application For Active Control System. In *2021 7th International Conference on Hydraulic and Civil Engineering & Smart Water Conservancy and Intelligent Disaster Reduction Forum (ICHCE & SWIDR)*; IEEE, 2021; pp. 478–486.
- (18) Yu, Z.; Centola, M.; Valero, J.; Matthies, M.; Šulc, P.; Famulok, M. A self-regulating DNA rotaxane linear actuator driven by chemical energy. *J. Am. Chem. Soc.* **2021**, *143*, 13292–13298.
- (19) Klute, G. K.; Czerniecki, J. M.; Hannaford, B. Artificial muscles: Actuators for biorobotic systems. *Int. J. Rob. Res.* **2002**, *21*, 295–309.
- (20) Zhang, J.; Sheng, J.; O'Neill, C. T.; Walsh, C. J.; Wood, R. J.; Ryu, J.-H.; Desai, J. P.; Yip, M. C. Robotic artificial muscles: Current progress and future perspectives. *IEEE Trans. Rob.* **2019**, *35*, 761–781.
- (21) Wang, J.; Gao, D.; Lee, P. S. Recent progress in artificial muscles for interactive soft robotics. *Adv. Mater.* **2021**, *33*, 2003088.
- (22) Gao, Z.; Shi, Q.; Fukuda, T.; Li, C.; Huang, Q. An overview of biomimetic robots with animal behaviors. *Neurocomputing* **2019**, *332*, 339–350.
- (23) Cho, K.-J.; Wood, R., Biomimetic robots. In *Springer handbook of robotics*; Springer, 2016; pp. 543–574.
- (24) Sun, L.; Huang, W. M.; Wang, C. C.; Ding, Z.; Zhao, Y.; Tang, C.; Gao, X. Y. Polymeric shape memory materials and actuators. *Liq. Cryst.* **2014**, *41*, 277–289.
- (25) Hamidullah, M.; Élie-Caille, C.; Leblois, T. Higher-order Lamb waves with quasi-zero surface displacement components on a GaAs piezoelectric plate. *J. Phys. D: Appl. Phys.* **2022**, *55*, No. 094003.
- (26) Latour, A.; Gras, A.; Pawlak, S., Method for manufacturing a plastic part forming a human-machine control interface. United States patent application US 16,530,601, 2020.
- (27) Tahara, K.; Hayashi, R.; Masuya, K.; Takagi, K.; Irisawa, T.; Yamauchi, T.; Tanaka, E. Rotational angle control of a twisted polymeric fiber actuator by an estimated temperature feedback. *IEEE Rob. Autom. Lett.* **2019**, *4*, 2447–2454.
- (28) Etches, J. A.; Bond, I. P. Development of an actuator based on ionic epoxy gel polymer. *Smart Mater. Struct.* **2011**, *20*, No. 045020.
- (29) Hubbard, A. M.; Cui, W.; Huang, Y.; Takahashi, R.; Dickey, M. D.; Genzer, J.; King, D. R.; Gong, J. P. Hydrogel/elastomer laminates bonded via fabric interphases for stimuli-responsive actuators. *Matter* **2019**, *1*, 674–689.
- (30) Štular, D.; Kruse, M.; Župunski, V.; Kreinest, L.; Medved, J.; Gries, T.; Blaeser, A.; Jerman, I.; Simončič, B.; Tomšič, B. Smart Stimuli-Responsive Poly(lactic Acid)-Hydrogel Fibers Produced via Electrospinning. *Fibers Polym.* **2019**, *20*, 1857–1868.
- (31) Di, J.; Zhang, X.; Yong, Z.; Zhang, Y.; Li, D.; Li, R.; Li, Q. Carbon-nanotube fibers for wearable devices and smart textiles. *Adv. Mater.* **2016**, *28*, 10529–10538.
- (32) Zagorodko, O.; Melnyk, T.; Rogier, O.; Nebot, V. J.; Vicent, M. J. Higher-order interfiber interactions in the self-assembly of benzene-1,3,5-tricarboxamide-based peptides in water. *Polym. Chem.* **2021**, *12*, 3478–3487.
- (33) Zheng, Q.; Jiang, Z.; Xu, X.; Xu, C.; Zhu, M.; Chen, C.; Fu, F. Bio-inspired bicomponent fiber with multistimuli response to infrared light and humidity for smart actuators. *ACS Appl. Polym. Mater.* **2021**, *3*, 3131–3141.
- (34) Chen, H.; Ye, S.; Tao, Q.; Chen, Z.; Tu, Y.; Yang, X. Hygroresponsive Torsional Yarns and Actuators Based on Cascade Amplification of the Deformation. *Macromol. Mater. Eng.* **2021**, *306*, 2000822.
- (35) An, Y.; Gao, L.; Wang, T. Graphene oxide/alginate hydrogel fibers with hierarchically arranged helical structures for soft actuator application. *ACS Appl. Nano Mater.* **2020**, *3*, 5079–5087.
- (36) Hagler, J. E.; Peterson, B.; Murphy, A.; Leger, J. Silk-polyppyrrrole biocompatible actuator performance under biologically relevant conditions. *Bull. Am. Phys. Soc.* **2017**, 62.
- (37) Lan, W.; He, L.; Liu, Y. Preparation and properties of sodium carboxymethyl cellulose/sodium alginate/chitosan composite film. *Coatings* **2018**, *8*, 291.
- (38) Jeong, D.; Kim, C.; Kim, Y.; Jung, S. Dual crosslinked carboxymethyl cellulose/polyacrylamide interpenetrating hydrogels with highly enhanced mechanical strength and superabsorbent properties. *Eur. Polym. J.* **2020**, *127*, No. 109586.
- (39) Li, H.; Wang, H.; Zhang, D.; Xu, Z.; Liu, W. A highly tough and stiff supramolecular polymer double network hydrogel. *Polymer* **2018**, *153*, 193–200.
- (40) Kamthai, S.; Magaraphan, R. Mechanical and barrier properties of spray dried carboxymethyl cellulose (CMC) film from bleached bagasse pulp. *Ind. Crops Prod.* **2017**, *109*, 753–761.
- (41) Sasso, C.; Zeno, E.; Petit-Conil, M.; Chaussy, D.; Belgacem, M. N.; Tapin-Lingua, S.; Beneventi, D. Highly conducting polypyrrole/cellulose nanocomposite films with enhanced mechanical properties. *Macromol. Mater. Eng.* **2010**, *295*, 934–941.
- (42) Wang, Z.; Wang, M.; Ma, M.-m.; Zhang, N. Water-Resistant and Stretchable Conductive Ionic Hydrogel Fibers Reinforced by Carboxymethyl Cellulose. *Chin. J. Chem. Phys.* **2021**, *134012*, 1674–0068.
- (43) Liu, D.; Tarakanova, A.; Hsu, C. C.; Yu, M.; Zheng, S.; Yu, L.; Liu, J.; He, Y.; Dunstan, D. J.; Buehler, M. J. Spider dragline silk as torsional actuator driven by humidity. *Sci. Adv.* **2019**, *5*, No. eaau9183.